Research Article

Ans Al Rashid*, Sumama Nuthana Kalva, Mokarram Hossain, and Muammer Koç

Cobalt iron oxide-infused silicone nanocomposites: Magnetoactive materials for remote actuation and sensing

https://doi.org/10.1515/ntrev-2025-0194
received March 3, 2025; accepted June 6, 2025

Abstract: Magnetoactive polymer composites (MAPCs) are promising smart materials owing to their shape-changing behaviour in response to magnetic fields. MAPCs find promising niches in several applications, including soft robotics, sensors, biomedical implants, smart prosthetics, and flexible electronics. Although several works have reported the synthesis of magnetic-responsive polymer composites, this work utilizes highly magnetic nanoparticles (*i.e.* cobalt iron oxide) to produce extremely soft MAPCs. Novel MAPCs were developed using room-temperature vulcanizing (RTV) silicone rubber as the base matrix, incorporating cobalt iron oxide ($CoFe_2O_4$, referred to as CIO) nanoparticles as the magnetic filler. Varying concentrations of CIO nanoparticles (0.25, 0.5, 1, and 3%) were used to synthesize isotropic and anisotropic MAPCs. Silicone/CIO MAPCs were characterized for their microstructural, thermal, mechanical, and magnetic properties. An increase in the CIO nanoparticle concentration within the silicone matrix resulted in an improved mechanical performance, where a compressive modulus of 0.199 MPa for silicone/0.25% CIO improved to 0.340 MPa for silicone/3% CIO. Likewise, an improved tensile strength was observed due to particle alignment, resulting in an increase from 1.25 MPa (for isotropic samples) to 1.356 MPa (for anisotropic samples) in silicone/1% CIO MAPCs. Silicone/CIO MAPCs also revealed a higher failure strain than pure silicone samples. Finally, an improvement in the magnetic properties of MAPCs was observed with increasing CIO concentrations, where increased saturation magnetization from 0.087 to 1.057 EMU/g and remanence from 0.054 to 0.625 EMU/g were recorded with an increase in CIO content from 0.25 to 3% in the silicone matrix. The silicone/CIO composites exhibited suitable magnetic responsiveness and mechanical characteristics that make them promising materials for applications in remote actuation and sensing.

Keywords: MAPCs, soft materials, magnetic response, remote sensing, actuation

1 Introduction

Magnetoactive polymer composites (MAPCs) have emerged as a class of smart materials capable of responding to external magnetic fields, enabling dynamic control over their mechanical properties [1–3]. These materials consist of a polymer matrix integrated with magnetic particles, offering a combination of polymer flexibility and processability with the responsive properties of magnetic components [4–6]. MAPCs can be classified based on the types of polymer matrices and the nature of the magnetic fillers used [7,8]. MAPCs can be broadly categorized into two main categories: magnetostrictive and magnetorheological polymer composites. Magnetostrictive composites are loaded with magnetic fillers that physically deform under a magnetic field, causing the entire material to bend or twist [9,10]. On the other hand, magnetorheological composites contain magnetic particles dispersed within a polymer matrix [11,12]. When a magnetic field is applied, particles align and significantly alter the rheological and mechanical (*e.g.* stiffness) properties of the composite [13]. It is essential to distinguish MAPCs from magnetorheological elastomers (MREs), a specific type of MAPC utilizing elastomeric polymers. Magnetoactive hydrogels represent a unique class of materials in which the polymer matrix is substituted with a water-based hydrogel [14–16]. Furthermore, MAPCs are also categorized based on the distribution of the magnetic particles within the polymer matrix, which can either be aligned in a desired

*** Corresponding author: Ans Al Rashid**, Division of Sustainable Development, College of Science and Engineering, Hamad Bin Khalifa University, Qatar Foundation, Doha, 34110, Qatar,
e-mail: aalrashid@hbku.edu.qa, ans.ravian@gmail.com
Sumama Nuthana Kalva, Muammer Koç: Division of Sustainable Development, College of Science and Engineering, Hamad Bin Khalifa University, Qatar Foundation, Doha, 34110, Qatar
Mokarram Hossain: Zienkiewicz Institute for Modelling, Data and AI, Faculty of Science and Engineering, Swansea University, Swansea, SA1 8EN, United Kingdom

direction or can be randomly oriented to produce anisotropic or isotropic MAPCs [17].

Polymer matrices can range from elastomers, such as silicones and polyurethanes, to thermoplastics and thermosets, each offering different mechanical properties [18]. The magnetic fillers are typically metallic particles, such as iron, cobalt, or nickel, or their oxides, including magnetite (Fe_3O_4) and cobalt iron oxide ($CoFe_2O_4$, referred to as CIO) [19,20]. The choice of the polymer and magnetic filler significantly influences MAPCs' behaviour, including their magneto-mechanical response, durability, and potential applications [21,22]. Silicone, with its excellent elasticity, chemical stability, and biocompatibility, is a popular choice as a matrix material [23]. Meanwhile, CIO is favoured as a filler for its high magnetic coercivity and stability, making it particularly suitable for applications requiring strong and reliable magnetic responsiveness [24].

Numerous studies have explored the influence of various materials and their compositions on the magnetic responsiveness of MAPCs. For instance, Horváth and Szalai [25] examined the influence of various magnetic particles (iron and magnetite) and their arrangement within a silicone rubber-based MRE. Therein, it was revealed that MREs with magnetite responded faster (1.2 to 12.1 ms) than iron-filled ones (4.0 to 60.5 ms) due to magnetite-induced crosslinking effects. Anisotropic particle structures within the MRE also improved response time, although residual magnetism could hinder this benefit. Balogh *et al.* [26] investigated how different magnetic fillers (magnetite and iron) affect the deformation of rubbery MRE discs under a magnetic field. All MREs expanded in the field direction, while the amount of expansion depends on the filler type and concentration.

In contrast to classical MREs using soft-magnetic particles such as iron oxides, Moreno-Mateos *et al.* [27] explored a new type of MRE using hard-magnetic particles. Stepanov *et al.* [28] also studied rubbery MREs filled with permanent magnets (*e.g.* NdFeB) instead of the usual soft-magnetic particles. Unlike traditional MREs requiring a constant magnetic field for stiffness change, the developed "hard-magnetic MREs" maintained stiffness even after turning off the magnetic field. Made with a very soft rubber matrix, these MREs stiffened significantly under a magnetic field and exhibited interesting shape-changing properties due to the interaction between the permanent magnets and the soft matrix, offering potential advantages for applications where long-lasting stiffness control is desired. Lee *et al.* [29] improved the magnetic response of MREs by adding rod-shaped magnetic nanoparticles (gamma-ferrite) to a composite filled with iron particles and natural rubber (CV-60). This combination increased the stiffening effect of the MRE under a magnetic field by about 25% compared to MREs with only iron particles.

Rahmatabadi *et al.* [30] developed Fe_3O_4-reinforced polyethylene terephthalate glycol (PETG) nanocomposites for enhanced shape memory effect utilizing thermo-magnetic responsiveness. They utilized the melt mixing technique for nanocomposite synthesis, followed by mechanical and morphological investigations on the 3D-printed samples. Incorporation of Fe_3O_4 nanoparticles resulted in improved dynamic mechanical, uniaxial, and shape memory of the composites, with 15% Fe_3O_4 concentration found optimal for a balanced mechanical strength and flexibility. In another study, Mirasadi *et al.* [31] used PETG and acrylonitrile butadiene styrene (ABS) blend as matrix and Fe_3O_4 nanoparticles to develop remotely driven shape memory composites. An increase in Fe_3O_4 nanoparticle concentrations improved the mechanical strength of 3D-printed composites; however, elongation was negatively affected, making the composites more brittle. Composites with 20% Fe_3O_4 nanoparticle content revealed an excellent shape memory effect under applied heat and magnetic fields, despite poor print qualities. Likewise, Yousefi *et al.* [32] explored poly(lactic acid) (PLA)-poly (butylene adipate-co-terephthalate) (PBAT) blends as a base matrix with Fe_3O_4 nanoparticles to develop MAPCs. A 10 wt% Fe_3O_4 nanoparticle was found to be optimal, and beyond this concentration, material performance and nanoparticle agglomeration were observed to be reduced. The unique ability of MAPCs to undergo shape change, stiffness modulation, and force generation under magnetic influence has made them an attractive choice for a wide range of advanced applications, particularly in soft robotics, flexible sensors [33–35], biomedical implants [15,36,37], vibrating damping and noise reduction [38–40], smart prosthetics [41,42], and flexible electronics [43–45], as illustrated in Figure 1.

The literature highlights a clear need for the development of innovative MAPCs tailored for remote actuation and sensing applications. As evident from the literature, previous studies have mainly utilized conventional fillers (mainly, iron oxide or ferrites); however, this study employs CIO nanoparticles, which are known for their superior magnetic properties. CIO nanoparticles also maintain the softness of the silicone matrix while improving the magnetic properties of the base material, *i.e.* silicone. To the best of our knowledge, no existing studies have investigated the synthesis of MAPCs using room-temperature vulcanizing (RTV) silicone rubber and CIO nanoparticles. The specific materials used in this study – silicone as the polymer matrix and CIO as the magnetic filler – bring their unique advantages to MAPC design. Silicone is widely used in applications requiring flexibility, durability, and biocompatibility, including in medical devices, wearable electronics, and soft robotic systems. Its ability, on the one hand, to maintain elasticity over a wide range of temperatures and environments makes it an ideal matrix for

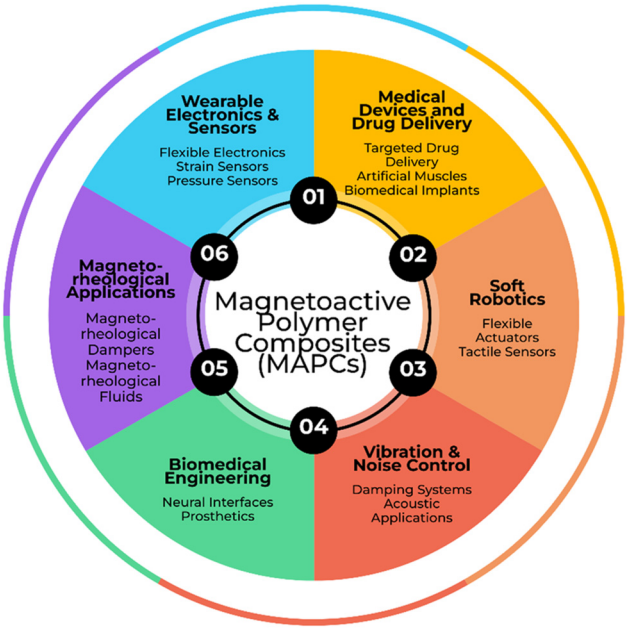

Figure 1: Potential applications of MAPCs in medical devices and drug delivery (targeted drug delivery, artificial muscles, implants), soft robotics (flexible actuators, tactile sensors), vibration and noise control (damping systems, acoustics), biomedical (neural interfaces, prosthetics), magnetorheological (dampers, fluids), and wearable electronics and sensors (flexible electronics, strain, and pressure sensors).

MAPCs designed for harsh or variable conditions. Cobalt iron oxide, on the other hand, provides the composite with robust magnetic properties, essential for applications that demand precise and strong magnetic responses, such as in remote actuation and high-sensitivity sensing. The combination of these materials in an MAPC offers a versatile platform for developing advanced systems with enhanced performance in demanding applications. MAPCs were synthesized using a mechanical mixing approach with isotropic and anisotropic CIO nanoparticle distribution and were characterized for their microscopic, chemical, thermal, mechanical, and magnetic properties. The magnetic behaviour of the silicone/CIO nanocomposites indicated their potential suitability for remote actuation and sensing applications.

2 Materials and methods

2.1 Materials

RTV silicone, containing silicone and activator (separate), was purchased from Contenti (USA), with a specific gravity of 1.1, a tensile strength of 4.6 MPa, and a hardness of 28 Shore A, as per the manufacturer's product details. Cobalt iron oxide ($CoFe_2O_4$, abbreviated as CIO) nanoparticles, averaging 30 nm in size with 99% purity, and silicone oil (SO) with a viscosity of 100 mPa s and a density of 0.967 g/mL, were obtained from Sigma Aldrich (USA). The raw materials were utilized as supplied, without any additional pre-processing or purification.

2.2 Silicone/CIO nanocomposite synthesis

Silicone/CIO MAPCs were prepared using the mechanical mixing method (illustrated in Figure 2), a widely recognized technique for producing stable and homogeneously reinforced polymer composites [46,47]. Four compositions were formulated by varying the nanoparticle weight percentages (0.25, 0.5, 1, and 3%). CIO nanoparticles were incrementally introduced into 10 mL of SO in a glass beaker under continuous mechanical stirring. The SO/CIO solution was mixed for 15 min to achieve the homogenous dispersion of the nanoparticles within the SO. Mechanical mixing was employed as the preliminary dispersion step, which allowed the coarse but uniform CIO nanoparticle distribution within the SO, ensuring the appropriate wetting of CIO nanoparticles by SO and resulting in a homogenous starting mixture. Followed by an ultrasonication process for 5 min, which allowed the breaking of CIO nanoparticles agglomerates through high-frequency energy, further improving the dispersion. SO allowed a stable suspension of CIO nanoparticles for a homogenous dispersion within the silicone matrix. The synergic effect of both techniques, *i.e.* mechanical mixing and ultrasonication, significantly contributed to the enhanced dispersion of CIO nanoparticles, which affected the mechanical and magnetic properties of MAPCs, as discussed in the subsequent sections. The pre-defined weight of silicone (as detailed in Table 1) was added to another glass beaker. The prepared SO/CIO solution was then mixed thoroughly with the silicone base through rigorous mechanical mixing for 30 min to obtain a silicone/SO/CIO mixture. Finally, a curing agent (activator) was added to the mixture as prescribed by the manufacturer (10:1 weight ratio with respect to silicone), and mechanically mixed for another 15 min for a homogenous mixing of the crosslinking agent. The curing agent contains a tin-based catalyst that facilitates the crosslinking reaction between hydroxyl-terminated polysiloxane chains and silane functional groups. The curing process occurs at room temperature and releases alcohol as a byproduct, characteristic of condensation-type curing.

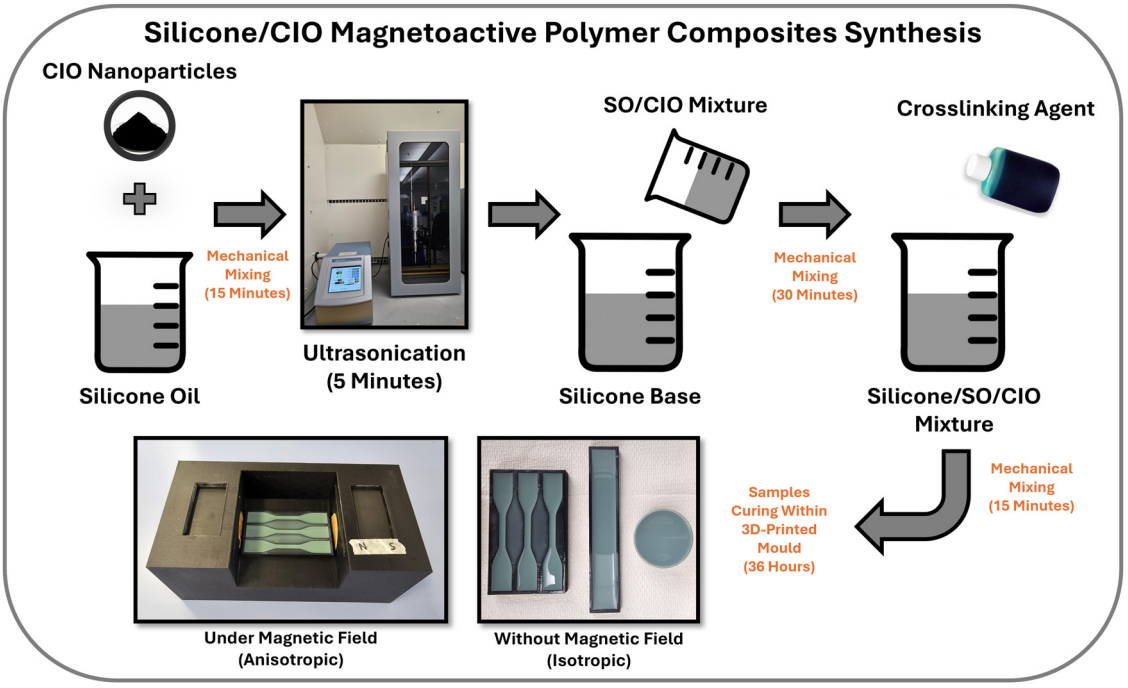

Figure 2: The synthesis process of silicone/CIO MAPCs involves the mixing of CIO nanoparticles in SO (mechanical mixing) followed by ultrasonication. The resulting mixture was added to the silicone base (mechanical mixing) followed by the addition of a crosslinking agent. The final mixture was poured into moulds for curing with (for anisotropic samples) and without (for isotropic samples) a magnetic field.

The final solution was then poured into a 3D-printed mould for curing to produce specimens for testing. The mould was designed using Solidworks to produce samples for tensile testing and magnetic actuation response of silicone/CIO MAPCs, followed by 3D-printing of it using Markforged Mark Two 3D printer using Onyx® material (from Markforged, USA). The silicone/CIO MAPCs were then left at room temperature for 36 h to cure completely. Compression testing specimens were prepared using Petri dishes to produce the disc samples measuring 33.5 mm in diameter and 9.5 mm in height. Silicone/CIO MAPC samples were then removed from the mould for chemical, thermal, mechanical, and magnetic characterization.

2.3 Magnetization of MAPCs

A custom setup was designed and 3D-printed for the magnetization of MAPCs (as reported in Figure 3). This setup was also 3D-printed using a Markforged Mark Two 3D printer using Onyx® material (from Markforged, USA). The setup contains slots for placing two permanent magnets (N42 neodymium disc magnets with a diameter of 2 in, a thickness of 0.5 in, and an approximate pull force of 87.5 lb) on each side and a platform for sample placement during the curing process to align the CIO nanoparticles along the magnetic field direction. The slots were secured with removable plates to avoid the magnet interaction with the surroundings.

Table 1: Composition of synthesized silicone/CIO MAPCs

Material	Silicone (wt%)	Silicone weight (g)			SO (mL)	CIO (wt%)	CIO weight (g)
		Silicone	Activator	Total			
Silicone	100	22.73	2.27	25.00	10 mL	—	—
Silicone/0.25% CIO	99.75	22.67	2.27	24.94		0.25	0.06
Silicone/0.50% CIO	99.50	22.61	2.26	24.87		0.50	0.13
Silicone/1% CIO	99	22.50	2.25	24.75		1	0.25
Silicone/3% CIO	97	22.05	2.20	24.25		3	0.75

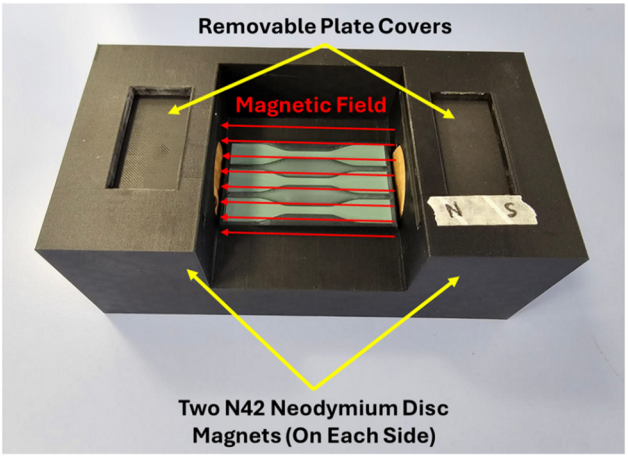

Figure 3: Custom-designed 3D-printed setup for magnetization of MAPCs contains two slots on either side for placement of permanent magnets (N42 neodymium disc magnets), and a platform between the magnets to place the mould during the curing process.

The setup allowed a homogenous magnetic field between the magnets with a magnetic field strength of 711 G at the centre and was used to produce anisotropic samples for tensile and magnetic actuation experiments. For each silicone/CIO MAPC composition, the moulds were placed in the magnetic fields during the curing process to produce anisotropic MAPCs; however, no magnetic field was applied to isotropic MAPCs. However, only isotropic samples were prepared for compression testing.

2.4 Material characterization

The morphology of silicone/CIO MAPCs was analysed using a field emission scanning electron microscope (FE-SEM, FEI Quanta650FEG) operated at an acceleration voltage of 20 kV and a working distance of 0.9 cm. SEM analysis assessed the dispersion of CIO nanoparticles and the influence of the applied magnetic field on anisotropic MAPCs. Fourier transform infrared (FTIR) spectroscopy was conducted on a Nicolet iS50 FT-IR spectrometer (Thermo Scientific, USA) equipped with an attenuated total reflectance (ATR) accessory featuring a diamond crystal plate. This technique was used to identify the molecular structure of MAPCs, utilizing 32 scans per sample in the 500–4,000 cm^{-1} spectral range with a resolution of 4 cm^{-1}. Thermal properties were investigated through thermogravimetric analysis (TGA) and differential scanning calorimetry (DSC) using a Thermal Analyzer (SDT 650, TA Instruments, USA). The silicone/CIO MAPCs were carefully placed in a ceramic crucible and heated from 30 to 900°C at a constant rate of 10°C/min under a nitrogen atmosphere.

2.5 Mechanical testing

Tensile testing specimens for silicone/CIO MAPCs were mould-cast according to ASTM D638 Type-IV standards [48]. Fully cured tensile testing specimens are reported in Figure 4(a). Tensile testing was performed using a Mark 10 material testing machine with a 250 N load cell at a 500 mm/min displacement rate. At least three samples were tested for each material composition and particle orientation (*i.e.* isotropic and anisotropic) to evaluate the impact of CIO nanoparticle concentration and their orientation on the mechanical response of MAPCs. Load *vs* displacement data were post-processed to evaluate stress *vs* strain behaviour. Compression testing specimens were

Figure 4: Fully cured silicone/CIO MAPC samples at different CIO nanoparticle concentrations. (a) Dog-bone-shaped samples for tensile testing and (b) disc samples for compression testing.

prepared using Petri dishes to produce the disc samples measuring 33.5 mm in diameter and 9.5 mm in height, as shown in Figure 4(b). Compression testing was also performed using a Mark 10 material testing machine with a 250 N load cell at a 2 mm/min displacement rate.

2.6 Magnetic properties and actuation response of MAPCs

The magnetic properties of silicone/CIO MAPCs were analysed using a vibrating sample magnetometer (VSM, Quantum Design Dynacool PPMS) within a magnetic field range of 0–10 kOe at room temperature. Hysteresis loops were recorded for all samples to determine the values of saturation magnetization (M_s), coercivity (H_c), and remanence (M_r). To evaluate the magnetic actuation response, silicone/CIO MAPCs were tested in the form of mould-cast strips with dimensions of 70 mm × 15 mm × 2 mm. MAPC strips were clamped at one end and placed vertically, hanging (free at the other end) to apply an external magnetic stimulus. N42 Neodymium disc magnet of 2 in. diameter and 1 in. thickness with a flux density (Br) of 13,150 G was used to actuate the MAPC strips. The magnet position was adjusted manually to record the threshold (1 mm), 5 mm, and 10 mm actuation in response to the applied magnetic field for each MAPC composition and configuration (isotropic and anisotropic). The distance (x) of the magnet from the strip was recorded for each actuation displacement, and the magnetic field (B_x) at a distance x from the magnet was calculated using the following equation [49,50]:

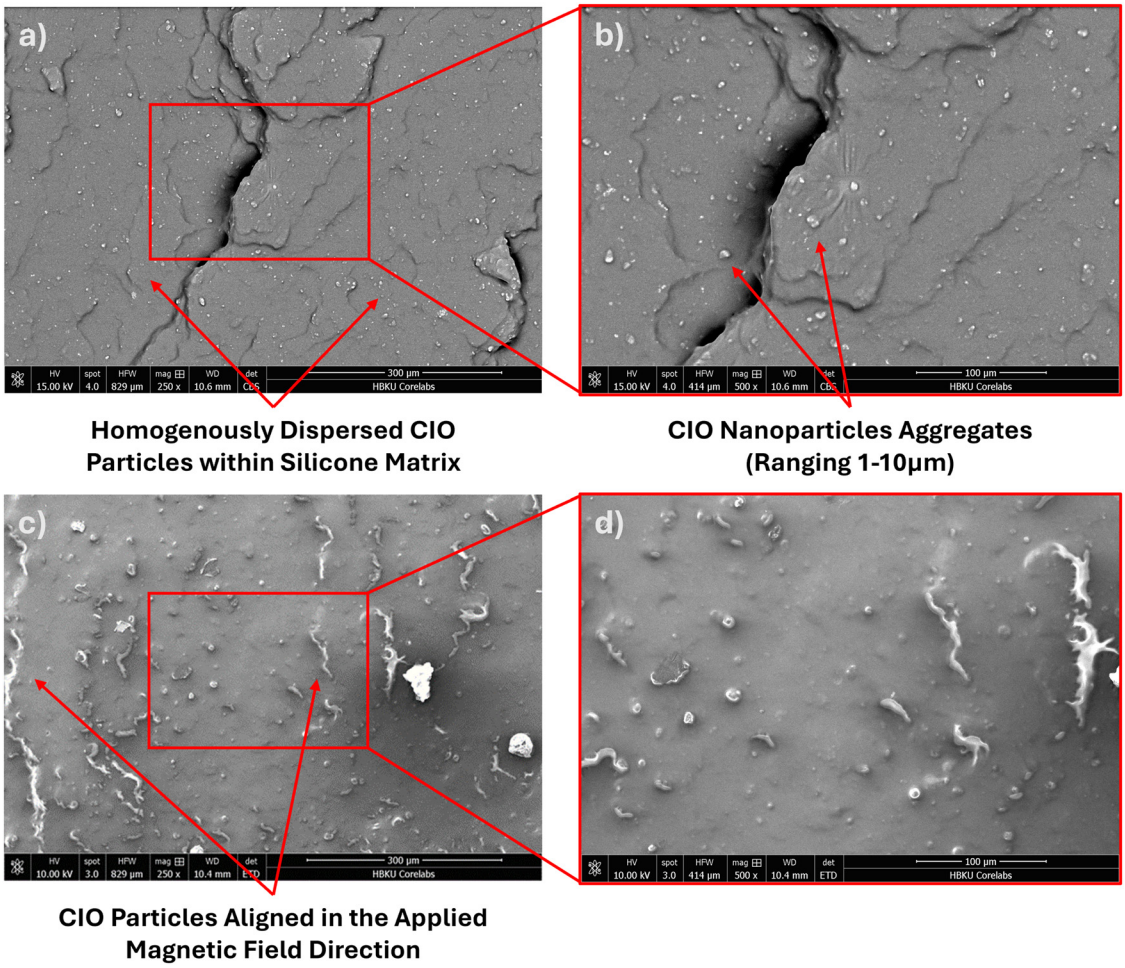

Figure 5: SEM analysis. (a) Silicone/1% CIO MAPCs (isotropic configuration) analysed at 250× magnification. (b) Silicone/1% CIO MAPCs (isotropic configuration) analysed at 500× magnification shows homogenously dispersed CIO particles within silicone matrix with some aggregates (ranging from 1–10 µm). (c) Silicone/1% CIO MAPCs (anisotropic configuration) analysed at 250× magnification. (d) Silicone/1% CIO MAPCs (anisotropic configuration) analysed at 500× magnification shows CIO nanoparticles aligned in the applied magnetic field direction.

$$B_x = \frac{B_r}{2}\cdot\left[\frac{T+x}{\sqrt{R^2+(T+x)^2}} - \frac{x}{\sqrt{R^2+x^2}}\right], \quad (1)$$

where T is the magnet thickness and R is the magnet radius.

3 Results and discussion

3.1 Scanning electron microscopy (SEM)

SEM was conducted on silicone/1% CIO MAPCs in both isotropic and anisotropic configurations to examine the dispersion of CIO nanoparticles within the silicone matrix and assess the effects of magnetic field-assisted curing. Before analysis, samples were coated with a 10 nm layer of gold to enhance surface conductivity for both surface and cross-sectional imaging. Due to the relatively low concentration of CIO nanoparticles (1%) in the MAPCs, only a limited number of nanoparticles were detected on the surface of the samples. However, the cross-sectional images provided clearer insights into the distribution of CIO nanoparticles, as illustrated in Figure 5. For the isotropic MAPCs, SEM images (Figure 5(a) and (b)) revealed a uniform and homogenous dispersion of CIO particles throughout the silicone matrix with some aggregates (ranging from 1 to 10 μm). These aggregates disrupt the uniform stress distribution within the silicone matrix and act as stress concentrators, negatively impacting the mechanical performance of MAPCs, especially at higher concentrations, *i.e.* 3%. In contrast, the anisotropic MAPCs (Figure 5(c) and (d)) exhibited alignment of the CIO nanoparticles along the direction of the applied magnetic field during curing, confirming the magnetic field's influence on the nanoparticle orientation within the matrix.

3.2 FTIR spectroscopy

FTIR spectroscopy was used to investigate the chemical structure and functional groups of pure silicone and

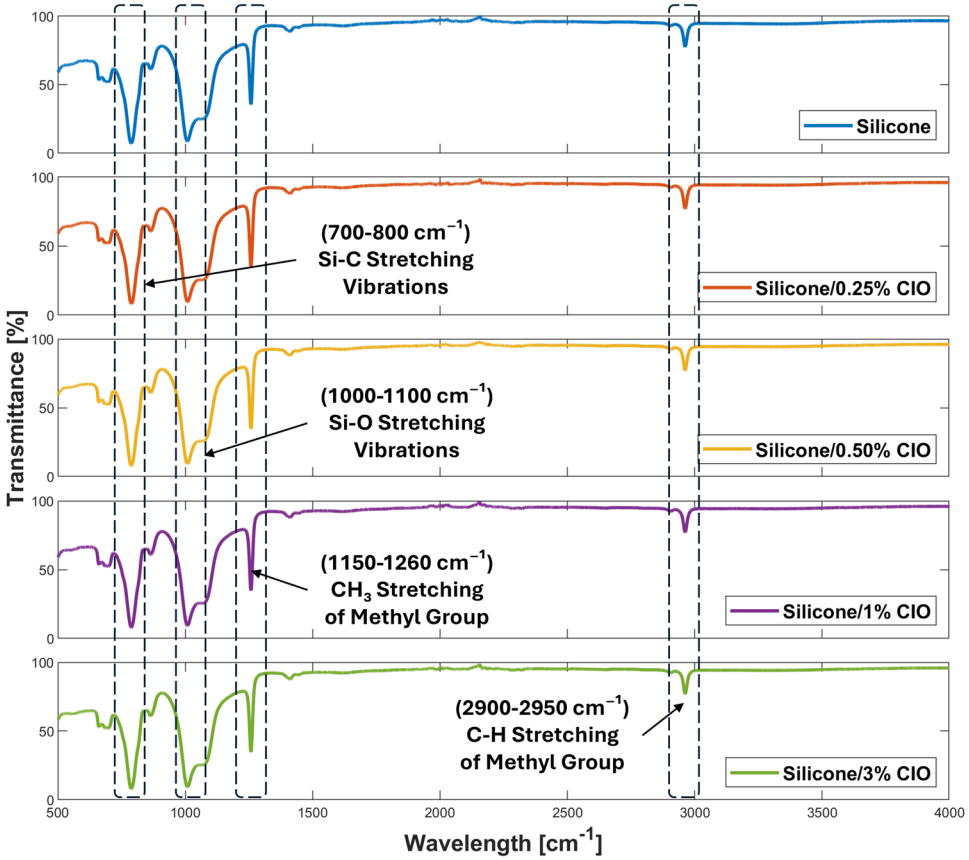

Figure 6: FTIR spectra of pure silicone and silicone/CIO MAPCs show characteristic peaks of pure silicone recorded at around 700–800 cm^{-1} (Si–CH$_3$ stretching vibrations), 1,000–1,100 cm^{-1} (Si–O–Si stretching vibrations), 1,150–1,260 cm^{-1} (CH$_3$ stretching of methyl group), and 2,900–2,950 cm^{-1} (C–H stretching of methyl group). No significant changes in characteristic peaks were observed with the addition of CIO nanoparticles.

silicone-based MAPCs (for isotropic configuration – with randomly aligned nanoparticles) reinforced with CIO nanoparticles at varying concentrations (0.25, 0.50, 1, and 3%). The FTIR spectra were recorded within the wavenumber range of 500–4,000 cm^{-1}, and the results are presented in Figure 6.

The FTIR spectrum of pure silicone exhibited characteristic absorption peaks corresponding to its siloxane backbone and methyl groups. Notable peaks were observed around 700–800 cm^{-1} (attributed to Si–CH_3 stretching vibrations) and 1,000–1,100 cm^{-1} (attributed to Si–O–Si stretching vibrations), which are consistent with the typical structure of polydimethylsiloxane (PDMS). In addition, the characteristic peaks were observed at around 1,150–1,260 cm^{-1} (attributed to CH_3 stretching of methyl groups) and 2,900–2,950 cm^{-1} (attributed to C–H stretching of methyl groups). With the addition of CIO nanoparticles, no significant changes in the intensity and position of the characteristic silicone peaks were observed, likely due to the formation of weak physical or chemical bonds between the CIO nanoparticles and the silicone matrix. Moreover, no new significant peaks were observed in MAPCs, indicating that the CIO nanoparticles primarily interact with the existing silicone bonds without introducing new functional groups. FTIR analysis revealed that the absence of new functional groups indicates that the CIO nanoparticles are well-dispersed within the matrix and do not form new chemical bonds, making MAPCs promising for maintaining the chemical integrity of silicone while enhancing its mechanical and magnetic properties.

3.3 TGA

TGA shows that both pure RTV silicone and silicone/CIO MAPCs undergo a single-step thermal degradation process, with the weight reduction beginning around 300°C (Figure 7(a)). As the temperature increases beyond this point, a sharp and significant weight loss is observed, corresponding to the thermal degradation of the RTV silicone matrix, likely involving the breakdown of the siloxane backbone and organic groups. Despite the incorporation of CIO, there is no significant shift in the onset of degradation, indicating that the initial thermal stability of the silicone matrix is largely unaffected. The degradation process continues rapidly up to around 550–600°C, after which the weight stabilizes, leaving a substantial residual mass. This final residue is higher than typical for pure silicone, indicating the presence of inorganic CIO nanoparticles that do not decompose at high temperatures.

In the DSC analysis of RTV silicone and silicone/CIO MAPCs, the incorporation of CIO does not significantly shift the degradation onset temperature but influences the heat flow trends, as shown in Figure 7(b). As the temperature increases, a broad endothermic peak appears, which is typically associated with molecular relaxation or softening within the silicone matrix, reflecting increased chain mobility. This is followed by a noticeable exothermic peak at higher temperatures, suggesting additional crosslinking or post-curing reactions. The presence of the nanoparticles causes a slight shift of the thermal events towards higher temperatures compared to pure silicone, indicating a small improvement in thermal resistance. An increasing CIO

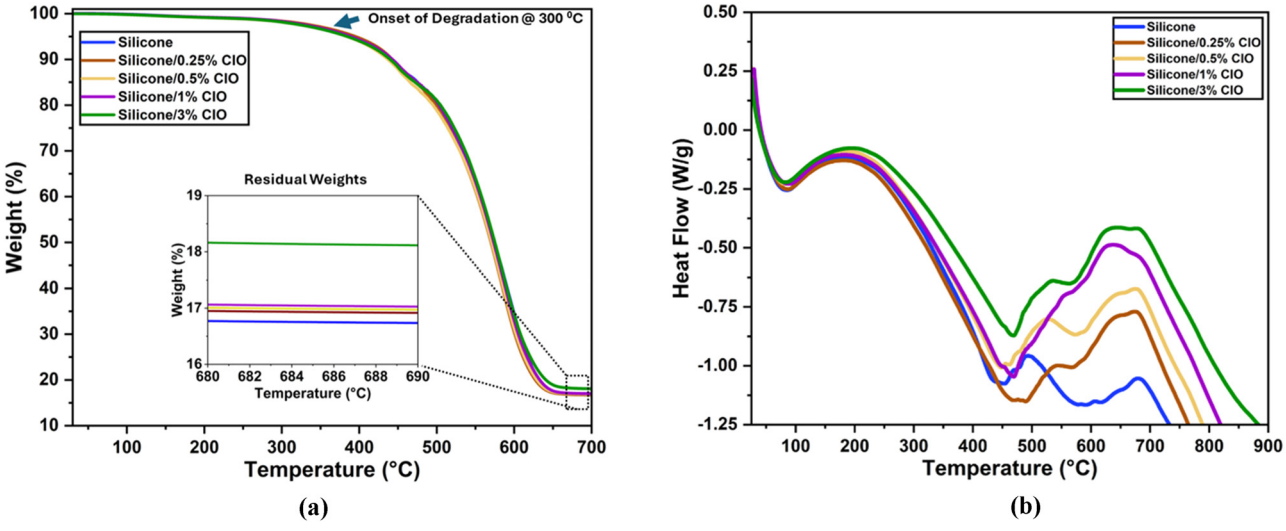

Figure 7: (a) TGA and (b) DSC of silicone and silicone/CIO MAPCs.

content intensifies these exothermic reactions, suggesting complex interactions between the CIO filler and the silicone matrix, which influence the material's thermal behaviour.

3.4 Mechanical testing

Mechanical properties of silicone/CIO MAPCs loaded with varying concentrations of CIO were evaluated under both compressive and tensile loading conditions, and the results are summarized in Table 2. Silicone/CIO MAPCs were tested for their compression modulus in isotropic configuration, while tensile strength, failure strain, and elastic modulus were measured in both isotropic and anisotropic configurations. The compressive behaviour of silicone/CIO MAPCs was evaluated until 25% of deformation relative to the initial sample height. In this range, all silicone/CIO MAPC compositions revealed a linear behaviour without any failure, as shown in Figure 8(a). The compression moduli of silicone/CIO MAPCs were measured from the slopes of these strain *vs* stress curves. The pure silicone sample exhibited a compression modulus of 0.412 MPa. With the addition of 0.25% CIO, the modulus decreased to 0.199 MPa, which might be due to weak interactions between the silicone matrix and the CIO nanofillers at low concentrations. As the CIO content increased from 0.50 to 3%, the compression modulus recovered, reaching 0.274, 0.322 and 0.340 MPa, for silicone/0.50% CIO, silicone/1% CIO, and silicone/3% CIO MAPCs, respectively, which indicates that higher CIO content improves the stiffness of silicone/CIO MAPCs due to better particle dispersion and increased silicone/CIO interaction. The stiffening effect at higher filler concentrations results from the reinforcing action of the magnetic nanoparticles, although the rate of increase slows down at higher CIO concentrations (*i.e.* 3%), potentially due to particle agglomeration.

Tensile testing was conducted on dog-bone-shaped specimens until failure, and displacement *vs* load data were post-processed to obtain strain *vs* stress curves, as shown in Figure 8(b) and (c). Figure 8(b) and (c) shows the strain *vs* stress behaviour of both isotropic and anisotropic silicone/CIO MAPCs. The tensile response of MAPCs followed a similar trend, as observed in compression testing, where an increase in the tensile strength was observed with increasing CIO content; however, the tensile strength decreased at 3% CIO concentration.

The tensile strength of pure silicone was observed to be around 1.356 MPa, whereas the addition of CIO nanoparticles reduced the tensile strength to 0.737 MPa for silicone/0.25% CIO. This reduction may be attributed to poor dispersion or weak interactions between the CIO particles and the silicone matrix at a low filler content. Further increasing the CIO concentrations resulted in improved tensile strength, *i.e.* 0.775 and 1.250 MPa for silicone/0.50% CIO and silicone/1% CIO, respectively. This improvement in the tensile strength can be attributed to the reinforcing effect of the CIO nanoparticles, which enhance the material's ability to resist deformation under tensile load. Finally, at a higher CIO concentration (*i.e.* 3%), the tensile strength decreases potentially due to nanoparticle agglomeration as a result of high loading, which can create stress concentration points and reduce the material's ability to resist tensile loads.

In the anisotropic samples, where the CIO particles were aligned in a magnetic field, the tensile strength was consistently higher compared to the isotropic counterparts, indicating the beneficial effect of particle alignment. Silicone/0.25% CIO MAPCs exhibited a tensile strength of 0.925 MPa, increasing to 0.975 MPa for the silicone/0.50% CIO and 1.356 MPa for the silicone/1% CIO, reflecting the improved load-bearing capacity provided by the alignment of CIO nanoparticles, which enhances stress transfer between the silicone matrix and CIO nanofillers. However, the tensile strength dropped to 0.857 MPa for the silicone/3% CIO, likely due to the same particle agglomeration effect observed in the isotropic configuration. Figure 8(d) presents a visual comparison of tensile strengths for isotropic and anisotropic silicone/CIO MAPCs.

Table 2: Summary of mechanical properties evaluated for silicone/CIO MAPCs obtained from tensile and compression tests

Material	Compression modulus (MPa)	Tensile strength (MPa)		Failure strain (mm/mm)		Elastic modulus (MPa)	
		Isotropic	Anisotropic	Isotropic	Anisotropic	Isotropic	Anisotropic
Silicone	0.412 ± 0.002	1.356 ± 0.03	—	11.875 ± 0.3	—	0.153 ± 0.003	—
Silicone/0.25% CIO	0.199 ± 0.005	0.737 ± 0.02	0.925 ± 0.04	14.167 ± 0.4	15.125 ± 0.5	0.065 ± 0.002	0.078 ± 0.003
Silicone/0.50% CIO	0.274 ± 0.001	0.775 ± 0.03	0.975 ± 0.05	12.667 ± 0.5	15.250 ± 0.6	0.081 ± 0.003	0.091 ± 0.005
Silicone/1% CIO	0.322 ± 0.004	1.250 ± 0.04	1.356 ± 0.05	12.042 ± 0.7	13.500 ± 0.8	0.141 ± 0.005	0.128 ± 0.007
Silicone/3% CIO	0.340 ± 0.006	1.031 ± 0.07	0.857 ± 0,08	12.459 ± 0.7	12.292 ± 0.8	0.109 ± 0.007	0.089 ± 0.008

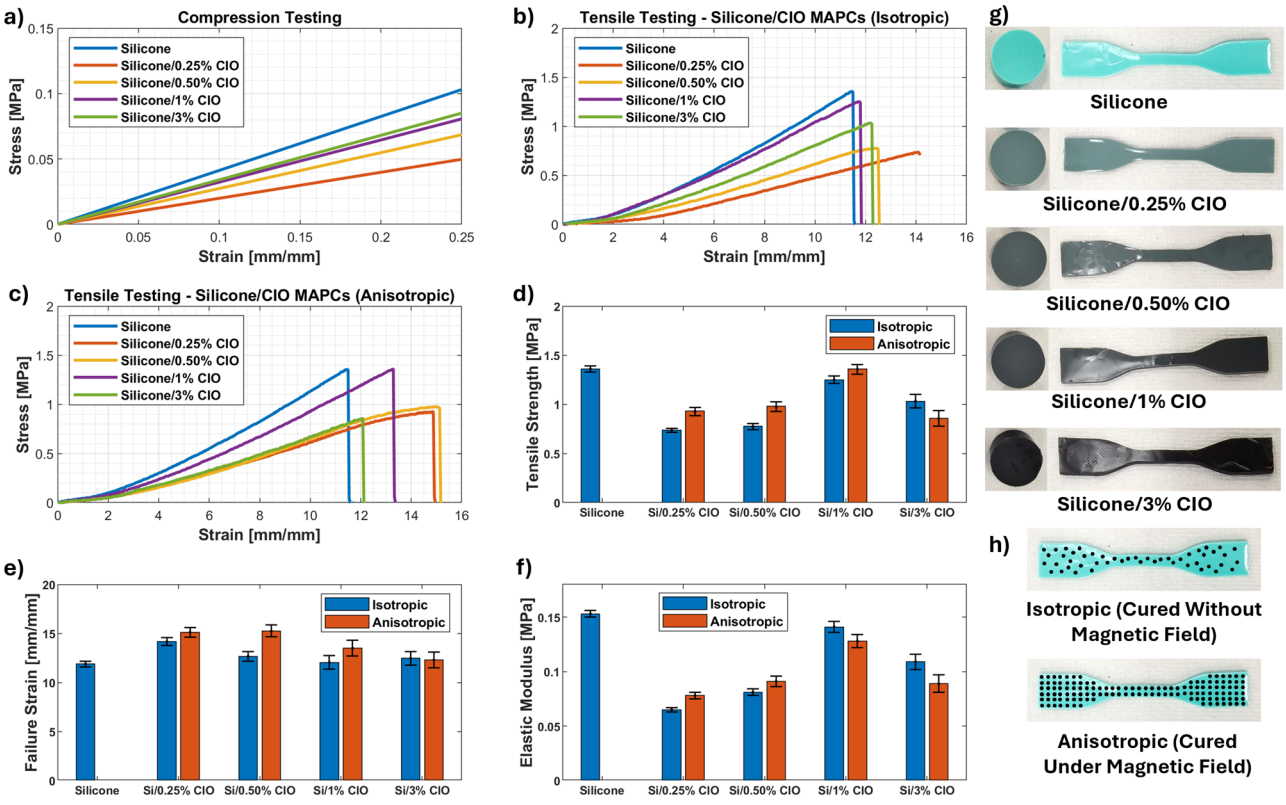

Figure 8: Mechanical properties of silicone/CIO MAPCs. (a) Strain *vs* stress curves for compression testing. (b) Strain *vs* stress curves for tensile testing of isotropic MAPCs. (c) Strain *vs* stress curves for tensile testing of anisotropic MAPCs. (d) Comparison of tensile strength for different materials and CIO nanoparticle orientation. (e) Comparison of failure strain for different materials and CIO nanoparticle orientation. (f) Comparison of tensile strength for different materials and CIO nanoparticle orientation. (g) Compression and tensile testing specimens. (h) Visual representation of CIO nanoparticles within isotropic and anisotropic MAPCs.

The failure strain, or elongation at break, of pure silicone was 11.88 mm/mm, as depicted in Figure 8(e). The failure strain increased to 14.17 mm/mm for the silicone/0.25% CIO, suggesting improved ductility at lower concentrations of nanoparticles, which could be due to the nanoparticles acting as spacers within the silicone matrix, allowing for more significant elongations before failure. Failure strain decreased with further increases in CIO concentrations, with 12.67, 12.04, and 12.46 mm/mm of failure strains for silicone/0.50% CIO, silicone/1% CIO, and silicone/3% CIO, respectively. In the anisotropic configuration, the failure strain was generally higher than in the isotropic configuration, indicating that the alignment of the CIO nanoparticles not only improves strength but also enhances the MAPCs' ability to deform under load. The silicone/0.50% CIO exhibited the highest failure strain (15.25 mm/mm), which decreased slightly as the CIO content increased, reaching 13.50 mm/mm for the silicone/1% CIO and 12.29 mm/mm for the silicone/3% CIO. The CIO nanoparticle alignment improves ductility; however, at higher CIO loadings, potential agglomerations can reduce the material's ability to deform before failure.

The elastic modulus, which reflects the stiffness of the material, was measured through uniaxial tensile tests performed on MAPCs, and for pure silicone, it was 0.153 MPa. Upon the addition of 0.25% CIO, the elastic modulus decreased to 0.065 MPa, likely due to weak interactions between the CIO nanoparticles and silicone matrix at low concentrations. However, as the CIO content increased, the modulus improved to 0.081 MPa for the silicone/0.50% CIO and 0.141 MPa for the silicone/1% CIO composite. The increased stiffness with higher CIO nanoparticle content is a result of the reinforcing effect, which restricts polymer chain mobility and enhances the material's resistance to deformation. For silicone/3% CIO, the modulus slightly decreased to 0.109 MPa, potentially due to particle agglomerations, which could create weak points in the MAPC structure. In the anisotropic configuration, the elastic modulus was improved for MAPCs at lower filler concentrations, as illustrated in Figure 8(f). Elastic modulus increased steadily with CIO content, reflecting the improved stiffness due to particle alignment. The silicone/0.25% CIO had an elastic modulus of 0.078 MPa, which

increased to 0.091 MPa for the silicone/0.50% CIO. The aligned particles likely restrict polymer chain mobility more effectively, resulting in a stiffer material. However, for silicone/1% CIO and silicone/3% CIO, the elastic modulus dropped slightly to 0.128 and 0.089 MPa, again likely due to agglomeration effects that reduce the efficiency of particle-matrix interactions.

As the CIO nanoparticle content increased, the tensile strength and elastic modulus generally improved up to 1% of CIO concentrations, reflecting the reinforcing role of CIO nanoparticles in the silicone matrix. The particles provide additional load-bearing capacity and restrict polymer chain mobility, leading to increased stiffness and strength. However, at higher concentrations (3% CIO), particle agglomeration likely occurred, which reduces the reinforcing effect and leads to a decrease in both tensile strength and elastic modulus. The anisotropic samples, where CIO nanoparticles were aligned using a magnetic field, consistently outperformed the isotropic samples in terms of tensile strength and elastic modulus up to 1% of CIO concentrations. The CIO nanoparticle alignment enhances stress transfer and load-bearing capacity, as the aligned nanoparticles can more effectively resist deformation and distribute applied loads. The alignment also improved failure strain, allowing for greater ductility before failure.

A key observation from the mechanical testing results is the trade-off between the tensile strength and failure strain. While the addition of CIO nanoparticles increases stiffness and strength, it also reduces the material's ability to deform, particularly at higher filler concentrations, which is a common phenomenon in reinforced polymers, where the increased stiffness typically comes at the cost of reduced ductility. At low CIO concentrations, poor particle dispersion likely weakens the silicone/CIO MAPCs, as observed in the low elastic modulus of the silicone/0.25% CIO. As the concentration increases, better dispersion

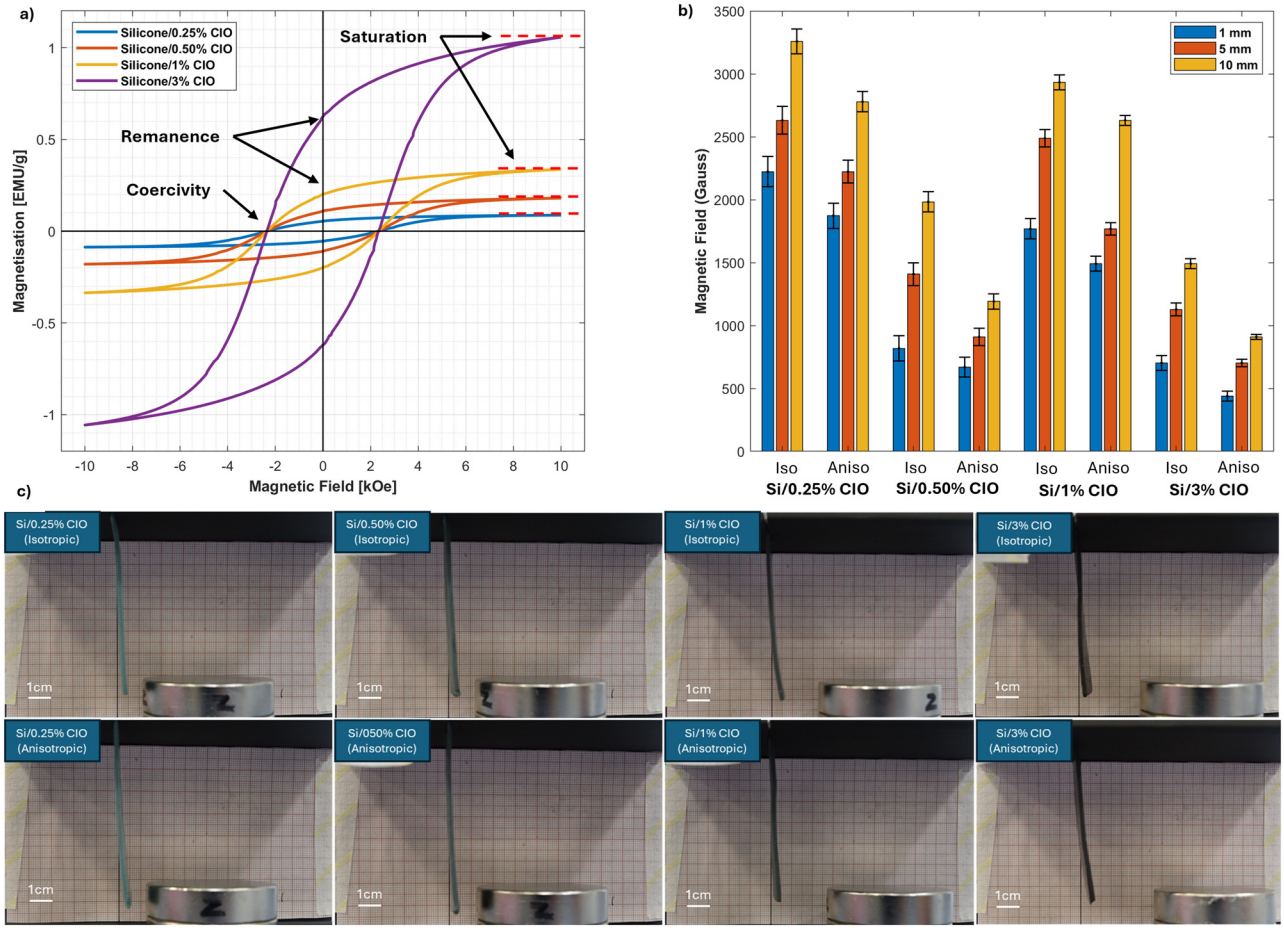

Figure 9: Magnetic properties and magnetic actuation response of silicone/CIO MAPCs. (a) Magnetic field *vs* magnetization profiles of silicone/CIO MAPCs represent an increased magnetic saturation and remanence with the increase in CIO nanoparticles concentration. (b) Magnetic field required to achieve threshold (1 mm), 5 mm, and 10 mm displacements for isotropic (iso) and anisotropic (aniso) configurations of silicone/CIO MAPCs. (c) Magnetic actuation of different configurations and compositions of silicone/CIO MAPCs.

enhances the mechanical properties, but beyond a certain threshold (*e.g.* 3% CIO), particle agglomeration occurs, which introduces stress concentration points and weakens the composites.

3.5 Magnetic properties of silicone/CIO MAPCs

Magnetic properties of the synthesized silicone/CIO MAPCs were evaluated using a VSM under the magnetic fields from 0 to 10 kOe at ambient temperature by recording the hysteresis loop and measuring saturation magnetization (M_s), coercivity (H_c), and remanence (M_r). The VSM results are illustrated in Figure 9(a) and summarized in Table 3. CIO nanoparticles, being ferromagnetic in nature, exhibit remarkable magnetic properties, including saturation magnetization (M_s) of 52.56 EMU/g, coercivity (H_c) of 2438 Oe, and remanence (M_r) of 30.8 EMU/g. For a detailed analysis of the magnetic properties of CIO nanoparticles, readers are referred to our previous study [51].

For silicone/CIO MAPCs, M_s increases with higher CIO content, demonstrating the proportional contribution of magnetic nanoparticles to the MAPCs' overall magnetization. H_c remains consistent, reflecting stable magnetic anisotropy and particle size distribution, with minimal influence from changes in CIO concentration. Finally, M_r increases with increasing CIO content due to stronger dipolar interactions. The saturation magnetization (M_s) of the MAPCs increased as the concentration of CIO nanoparticles in the matrix increased. The M_s values ranged from 0.087 EMU/g for the silicone/0.25% CIO to 1.057 EMU/g for the silicone/3% CIO due to the increasing amount of CIO nanoparticles embedded in the silicone matrix. As more CIO nanoparticles are incorporated, the overall magnetic moment of the MAPC increases due to the intrinsic magnetism of the CIO. The increase in M_s with CIO concentration follows the expected behaviour, where a higher content of magnetic nanoparticles results in a stronger collective magnetization under an external magnetic field, which indicates an effective dispersion of the nanoparticles within the matrix, allowing the magnetization to develop throughout the material without significant agglomeration, which could have otherwise reduced the magnetic response due to dipole–dipole interactions.

The coercivity (H_c) of MAPCs remained relatively constant across all materials tested, with values around 2350 Oe, indicating that the inclusion of different concentrations of CIO did not significantly alter the energy required to demagnetize the material. The stability of coercivity could be due to the particle size of CIO in the nanoscale regime contributing to a consistent coercivity, as the magnetization reversal mechanism does not drastically change with concentration. Furthermore, the intrinsic properties of CIO, such as its magneto-crystalline anisotropy, dominate the coercive behaviour. Thus, the MAPCs inherit this stability, with minimal influence from the polymer matrix or particle loading.

The remanent magnetization (M_r) also revealed a dependence on the CIO content, increasing from 0.054 EMU/g for the silicone/0.25% CIO to 0.625 EMU/g for the silicone/3% CIO. Remanence reflects the ability of the material to retain magnetization after the external magnetic field is removed. The increase in M_r suggests that with higher concentrations of CIO, the MAPCs retain a more significant magnetic moment due to the higher volume fraction of CIO nanoparticles, which is closely linked to the magnetic dipole–dipole interactions among nanoparticles. At lower concentrations, the nanoparticles are more isolated, and their interactions are weaker, leading to lower remanence. As the concentration increases, the nanoparticles are closer together, enabling stronger dipole–dipole interactions and leading to enhanced remanence. However, the lack of a sharp increase in M_r at higher CIO loading indicates that agglomeration effects might be limited, preventing excessive magnetic particle clustering, which could otherwise reduce the remanent magnetization by creating closed-loop magnetic domains.

The changes in magnetic properties can be attributed to dipolar interactions; as the CIO content increases, the magnetic dipoles within the material experience stronger

Table 3: Magnetic properties of the synthesized silicone/CIO MAPCs

Material	Saturation (M_s, EMU/g)	Coercivity (H_c, Oe)	Remanence (M_r, EMU/g)
CIO [51]	52.56	2,438	30.8
Silicone/0.25% CIO	0.087	2,350	0.054
Silicone/0.50% CIO	0.180	2,355	0.115
Silicone/1% CIO	0.336	2,351	0.202
Silicone/3% CIO	1.057	2,356	0.625

interactions, leading to higher magnetization (M_s and M_r). The increase in M_s and M_r is gradual and controlled, indicating uniform dispersion of CIO particles in the silicone matrix without significant agglomeration. In addition, nanoparticles typically exhibit surface spin disorder due to a large surface-to-volume ratio, which slightly reduces the total magnetization compared to bulk materials, especially at lower CIO concentrations. However, this effect is minimized at higher concentrations where collective magnetic behaviour dominates. Finally, the uniformity in coercivity (H_c) suggests that the particle size distribution and magnetic anisotropy of CIO nanoparticles are maintained across all MAPCs, resulting in stable coercive behaviour. This indicates that the synthesis and processing of the MAPCs achieved a consistent particle size and orientation, critical for reliable magnetic performance.

The synthesized silicone/CIO MAPCs outperformed similar materials reported in the literature in terms of their magnetic properties. Polyurethane (PU) nanocomposites with 3% magnetite nanoparticle (MNP) concentration revealed an M_s of 1.99 EMU/g, M_r of 0.033 EMU/g, and H_c of 15.37 Oe [49]. Another study reported an M_s of 1.719 EMU/g, M_r of 0.024 EMU/g, and H_c of 11.855 Oe for 3% magnetite nanoparticle-reinforced poly(butylene succinate-co-butylene adipate) (PBSA) MAPCs [50]. However, the M_s of silicone/CIO MAPCs reported in this study is lower than the similar materials (with the same nanoparticle concentrations, *i.e.* 3%) reported in the literature. The M_r and H_c for silicone/CIO MAPCs are significantly higher than the reported materials, indicating stronger magnetic retention and higher resistance to demagnetization, making them an excellent candidate for smart devices requiring precise control and sustained magnetic performance.

3.6 Magnetic actuation of silicone/CIO MAPCs

The magnetic actuation response of silicone/CIO MAPCs containing different concentrations of CIO nanoparticles (*i.e.* 0.25, 0.5, 1, and 3%) was investigated under isotropic and anisotropic configurations, as shown in Figure 9(b) and (c). Increasing the CIO concentration in both isotropic and anisotropic samples reduced the magnetic field required to achieve the same actuation distances (*i.e.* threshold (1 mm), 5 mm, and 10 mm), which indicates that a higher CIO content enhances the magnetic responsiveness of MAPCs due to stronger internal magnetic interactions. Silicone/0.25% CIO isotropic samples required 2,223 G to achieve a threshold (1 mm) displacement, increasing to 3258 G for 10 mm displacement. However, anisotropic samples needed lower fields (1769 G for 1 mm and 2,933G for 10 mm displacements). For silicone/0.50% CIO isotropic samples, the required magnetic field dropped further (1,873 G for 1 mm and 2,779 G for 10 mm displacements). As expected, anisotropic configurations revealed improved actuation efficiency, with lower magnetic fields (1,491 G for 1 mm and 2,631 G for 10 mm). A similar pattern was observed for silicone/1% CIO and silicone/3% CIO MAPCs, with the lowest magnetic fields observed in anisotropic samples (703G and 439 G for 1 mm for 1% CIO and 3% CIO, respectively). The reduction in required fields with increasing CIO content is due to enhanced magnetic interactions that facilitate actuation at lower applied magnetic fields. Therefore, a higher CIO content coupled with particle alignment significantly improved magnetic actuation efficiency, minimizing the magnetic field requirements for achieving desired displacements.

Across all silicone/CIO MAPCs, anisotropic samples consistently required lower magnetic fields than isotropic samples for the same actuation displacement owing to the alignment of magnetic nanoparticles along the direction of the magnetic field during sample preparation, facilitating more efficient magnetic actuation. The lower magnetic field requirements in anisotropic samples can be attributed to the alignment of particles, which provides a preferred pathway for the magnetic flux, reducing magnetic reluctance and allowing the MAPCs to respond more easily to the magnetic field. The difference in the magnetic field requirements between isotropic and anisotropic configurations decreased with increasing CIO content. At higher concentrations (1 and 3%), the magnetic interaction within the isotropic samples was strong enough to partially compensate for the lack of alignment, resulting in a less pronounced difference compared to lower concentrations. The magnetic actuation results highlight the importance of optimizing both the concentration and distribution of magnetic particles to enhance the performance of MAPCs for remote actuation applications.

4 Conclusions and future scope

In this study, MAPCs were developed using RTV silicone as the matrix material and cobalt iron oxide (CIO) nanoparticles as the magnetic filler, with concentrations of 0.25, 0.50, 1, and 3%. Silicone/CIO MAPCs were prepared through a mechanical mixing and ultrasonication process, and field emission (FE-SEM) analysis confirmed the effective incorporation of CIO nanoparticles into the polymer matrix.

FTIR results revealed no significant changes in the intensity and position of the characteristic silicone peaks, likely due to the formation of weak physical or chemical bonds between the CIO nanoparticles and the silicone matrix. Moreover, no new significant peaks were observed in MAPCs, indicating that the CIO nanoparticles primarily interact with the existing silicone bonds without introducing new functional groups. An increase in CIO nanoparticle concentration within the silicone matrix resulted in improved mechanical performance, where a compressive modulus of 0.199 MPa for silicone/0.25% CIO improved to 0.340 MPa for silicone/3% CIO. Likewise, an improved tensile strength was observed due to particle alignment, resulting in an increase from 1.25 MPa (for isotropic samples) to 1.356 MPa (for anisotropic samples) in silicone/1% CIO MAPCs. Silicone/CIO MAPCs also revealed higher failure strain than pure silicone samples. Finally, an improvement in the magnetic properties of MAPCs was observed with increasing CIO concentrations, where increased saturation magnetization from 0.087 to 1.057 EMU/g and remanence from 0.054 to 0.625 EMU/g were recorded with an increase in the CIO content from 0.25 to 3% in the silicone matrix. Silicone/1% CIO MAPCs were found to be optimum in terms of mechanical performance, while silicone/3% CIO MAPCs performed exceptionally well in terms of magnetic actuation and magnetic properties.

The primary challenge while dealing with nanoparticles and high-viscosity base polymers is homogenous dispersion, especially at higher concentrations, which could potentially impact the mechanical performance of the composites. More effective surfactants could be utilized to overcome this issue to improve the interaction of nanoparticles and the polymer matrix. In future research, the synthesized MAPCs will be transformed into feedstock materials, such as inks, for additive manufacturing techniques like direct ink writing. These advanced processes will enable the prototyping and testing of innovative design concepts, leveraging the flexibility offered in design and fabrication. This approach is expected to unlock new possibilities for these materials in remote actuation and sensing, broadening their potential applications.

Acknowledgments: The authors would like to acknowledge HBKU core labs for their support in the characterization of the samples. Open Access funding was provided by the Qatar National Library.

Funding information: M. Hossain acknowledges the support of the EPSRC via a Standard Grant (EP/Z535710/1) and the Royal Society (UK) through the International Exchange Grant (IEC/NSFC/211316).

Author contributions: A. Al Rashid and M. Koç: data curation; A. Al Rashid and S. N. Kalva: formal analysis, investigation, and writing, review and editing; A. Al Rashid: testing and methodology; A. Al Rashid and M. Hossain: project administration and writing – original draft; M. Koc: resources, supervision, and visualization. All authors have accepted responsibility for the entire content of this manuscript and approved its submission.

Conflict of interest: The authors state no conflict of interest.

Data availability statement: The datasets generated and/or analysed during the current study are available from the corresponding author on reasonable request.

References

[1] Li W, Gu H, Liu Z, Zhang H, Jiang L, Zhou X. Research progress in the synthesis and application of magnetic self-healing polymer composites. Eur Polym J. 2024;202:112633. doi: 10.1016/j.eurpolymj.2023.112633.

[2] Narayanan P, Pramanik R, Arockiarajan A. Hard magnetics and soft materials—A synergy. Smart Mater Struct. 2024;33:43001. doi: 10.1088/1361-665X/ad2bd8.

[3] Lalegani Dezaki M, Bodaghi M. Sustainable 4D printing of magneto-electroactive shape memory polymer composites. Int J Adv Manuf Technol. 2023;126:35–48. doi: 10.1007/s00170-023-11101-0.

[4] Afshari P, Pavlyuk M, Lira C, Katnam K-B, Bodaghi M, Yazdani Nezhad H. Mechanical strain tailoring via magnetic field assisted 3D printing of iron particles embedded polymer nanocomposites. Macromol Mater Eng. 2023;308:2300194. doi: 10.1002/mame.202300194.

[5] Tariq A, Arif ZU, Khalid MY, Hossain M, Rasool PI, Umer R, et al. Recent advances in the additive manufacturing of stimuli-responsive soft polymers. Adv Eng Mater. 2023;25:2301074. doi: 10.1002/adem.202301074.

[6] Khalid MY, Arif ZU, Tariq A, Hossain M, Ahmed Khan K, Umer R. 3D printing of magneto-active smart materials for advanced actuators and soft robotics applications. Eur Polym J. 2024;205:112718. doi: 10.1016/j.eurpolymj.2023.112718.

[7] Liu H, Wang F, Wu W, Dong X, Sang L. 4D printing of mechanically robust PLA/TPU/Fe_3O_4 magneto-responsive shape memory polymers for smart structures. Compos B Eng. 2023;248:110382. doi: 10.1016/j.compositesb.2022.110382.

[8] Garcia-Gonzalez D, Moreno MA, Valencia L, Arias A, Velasco D. Influence of elastomeric matrix and particle volume fraction on the mechanical response of magneto-active polymers. Compos B Eng. 2021;215:108796. doi: 10.1016/j.compositesb.2021.108796.

[9] Stolbov OV, Raikher YL. Magnetostrictive and magnetoactive effects in piezoelectric polymer composites. Nanomaterials. 2024;14(1):31. doi: 10.3390/nano14010031.

[10] Stepanov GV, Bakhtiiarov AV, Lobanov DA, Storozhenko PA. Magnetoresistivity and piezoresistivity of magnetoactive

elastomers. J Magn Magn Mater. 2023;587:171313. doi: 10.1016/j.jmmm.2023.171313.
[11] Bastola AK, Paudel M, Li L, Li W. Recent progress of magnetorheological elastomers: A review. Smart Mater Struct. 2020;29:123002. doi: 10.1088/1361-665X/abbc77.
[12] Silva JA, Gouveia C, Dinis G, Pinto AM, Pereira AM. Giant magnetostriction in low-concentration magnetorheological elastomers. Compos B Eng. 2022;243:110125. doi: 10.1016/j.compositesb.2022.110125.
[13] Moreno-Mateos MA, Hossain M, Steinmann P, Garcia-Gonzalez D. Hybrid magnetorheological elastomers enable versatile soft actuators. NPJ Comput Mater. 2022;8:162. doi: 10.1038/s41524-022-00844-1.
[14] Shou Y, Liu L, Liu Q, Le Z, Lee KL, Li H, et al. Mechano-responsive hydrogel for direct stem cell manufacturing to therapy. Bioact Mater. 2023;24:387–400. doi: 10.1016/j.bioactmat.2022.12.019.
[15] Cedillo-Servin G, Dahri O, Meneses J, van Duijn J, Moon H, Sage F, et al. 3D printed magneto-active microfiber scaffolds for remote stimulation and guided organization of 3D in vitro skeletal muscle models. Small. 2024;20:2307178. doi: 10.1002/smll.202307178.
[16] Roy A, Zhang Z, Eiken MK, Shi A, Pena-Francesch A, Loebel C. Programmable tissue folding patterns in structured hydrogels. Adv Mater. 2024;36(43):2300017. doi: 10.1002/adma.202300017.
[17] Bastola AK, Hossain M. The shape – morphing performance of magnetoactive soft materials. Mater Des. 2021;211:110172. doi: 10.1016/j.matdes.2021.110172.
[18] Gopinath S, Adarsh NN, Radhakrishnan Nair P, Mathew S. Recent trends in thermo-responsive elastomeric shape memory polymer nanocomposites. Polym Compos. 2023;44:4433–58. doi: 10.1002/pc.27464.
[19] Lu S, Wang M, Zhao Z. Recent advances and future developments in Fe-based amorphous soft magnetic composites. J Non Cryst Solids. 2023;616:122440. doi: 10.1016/j.jnoncrysol.2023.122440.
[20] Mishra S, Yadav MD. Magnetic nanoparticles: A comprehensive review from synthesis to biomedical frontiers. Langmuir. 2024;40:17239–69. doi: 10.1021/acs.langmuir.4c01532.
[21] Nam TH, Petríková I, Marvalová B. Effects of applied strain, magnetic field, and temperature on the compressive stress relaxation behavior of magneto-sensitive elastomers. Mech Time Depend Mater. 2024;28:917–36. doi: 10.1007/s11043-023-09654-4.
[22] Xian W, Zhan Y-S, Maiti A, Saab AP, Li Y. Filled elastomers: Mechanistic and physics-driven modeling and applications as smart materials. Polymers (Basel). 2024;16(10):1387. doi: 10.3390/polym16101387.
[23] Kumar V, Alam MN, Manikkavel A, Song M, Lee D-J, Park S-S. Silicone rubber composites reinforced by carbon nanofillers and their hybrids for various applications: A review. Polymers (Basel). 2021;13. doi: 10.3390/polym13142322.
[24] Haniffa MACM, Munawar K, Chee CY, Pramanik S, Halilu A, Illias HA, et al. Cellulose supported magnetic nanohybrids: Synthesis, physicomagnetic properties and biomedical applications-A review. Carbohydr Polym. 2021;267:118136. doi: 10.1016/j.carbpol.2021.118136.
[25] Horváth B, Szalai I. Magnetic susceptibility and response time of isotropic and structured magnetorheological elastomers. J Intell Mater Syst Struct. 2023;34:706–16. doi: 10.1177/1045389X221117489.
[26] Balogh D, Guba S, Horváth B, Szalai I. Magnetic field-induced deformation of isotropic magnetorheological elastomers. Magnetochemistry. 2022;8(11):146. doi: 10.3390/magnetochemistry8110146.
[27] Moreno-Mateos MA, Lopez-Donaire ML, Hossain M, Garcia-Gonzalez D. Effects of soft and hard magnetic particles on the mechanical performance of ultra-soft magnetorheological elastomers. Smart Mater Struct. 2022;31(6):065018. doi: 10.1088/1361-665X/ac6bd3.
[28] Stepanov GV, Chertovich AV, Kramarenko EY. Magnetorheological and deformation properties of magnetically controlled elastomers with hard magnetic filler. J Magn Magn Mater. 2012;324(21):3448–51. doi: 10.1016/j.jmmm.2012.02.062.
[29] Lee CJ, Kwon SH, Choi HJ, Chung KH, Jung JH. Enhanced magnetorheological performance of carbonyl iron/natural rubber composite elastomer with gamma-ferrite additive. Colloid Polym Sci. 2018;296:1609–13. doi: 10.1007/s00396-018-4373-0.
[30] Rahmatabadi D, Mirasadi K, Bayati A, Khajepour M, Ghasemi I, Baniassadi M, et al. 4D printing thermo-magneto-responsive PETG-Fe_3O_4 nanocomposites with enhanced shape memory effects. Appl Mater Today. 2024;40:102361. doi: 10.1016/j.apmt.2024.102361.
[31] Mirasadi K, Rahmatabadi D, Ghasemi I, Khodaei M, Baniassadi M, Bodaghi M, et al. 3D and 4D printing of PETG–ABS–Fe_3O_4 nanocomposites with supreme remotely driven magneto-thermal shape-memory performance. Polymers (Basel). 2024;16(10):1398. doi: 10.3390/polym16101398.
[32] Yousefi MA, Rahmatabadi D, Baniassadi M, Bodaghi M, Baghani M. 4D printing of multifunctional and biodegradable PLA-PBAT-Fe_3O_4 nanocomposites with supreme mechanical and shape memory properties. Macromol Rapid Commun. 2025;46:2400661. doi: 10.1002/marc.202400661.
[33] Liao Z, Zoumhani O, Boutry CM. Recent advances in magnetic polymer composites for BioMEMS: A review. Materials. 2023;16(10):3802. doi: 10.3390/ma16103802.
[34] Taccola S, Bakhshi H, Sanchez Sifuentes M, Lloyd P, Tinsley LJ, Macdonald J, et al. Dual-material aerosol jet printing of magneto-responsive polymers with in-process tailorable composition for small-scale soft robotics. Adv Mater Technol. 2024;9(22):2400463. doi: 10.1002/admt.202400463.
[35] Wang Z, Wu Y, Zhu B, Chen Q, Wang L, Zhao Y, et al. A magnetic soft robot with multimodal sensing capability by multimaterial direct ink writing. Addit Manuf. 2023;61:103320. doi: 10.1016/j.addma.2022.103320.
[36] Brito-Pereira R, Martins P, Lanceros-Mendez S, Ribeiro C. Polymer-based magnetoelectric scaffolds for wireless bone repair: The fillers' effect on extracellular microenvironments. Compos Sci Technol. 2023;243:110263. doi: 10.1016/j.compscitech.2023.110263.
[37] Mucolli A, Midmer A, Manolesos M, Aldosari S, Lira C, Yazdani Nezhad H. Low magnetic field induced extrinsic strains in multifunctional particulate composites: An interrupted mechanical strengthening in 3D-printed nanocomposites. J Compos Sci. 2024;8(6):231. doi: 10.3390/jcs8060231.
[38] Savelev DV, Glavan G, Burdin DA, Belyaeva IA, Fetisov LY, Shamonin M, et al. Enhancement of magnetoelectric effect in polymer composites at low resonance frequencies by operation in the transverse-transverse mode. J Magn Magn Mater. 2024;598:172020. doi: 10.1016/j.jmmm.2024.172020.
[39] Makarova LA, Alekhina IA, Khairullin MF, Makarin RA, Perov NS. Dynamic magnetoelectric effect of soft layered composites with a magnetic elastomer. Polymers (Basel). 2023;15(10):2262. doi: 10.3390/polym15102262.
[40] Perales-Martínez IA, Palacios-Pineda LM, Elías-Zúñiga A, Olvera-Trejo D, Del Ángel-Sánchez K, Cruz-Cruz I, et al. Magnetic and viscoelastic response of magnetorheological elastomers based on

a combination of iron nano- and microparticles. Polymers (Basel). 2023;15(18):3703. doi: 10.3390/polym15183703.
[41] Acharya B, Behera A, Moharana S, Behera S. State-of-the-art in textile polymer composites and applications. In: Moharana S, Sahu BB, Nayak AK and Tiwari SK, editors. Polymer composites: Fundamentals and applications. Singapore: Springer; 2024. p. 357–98. doi: 10.1007/978-981-97-2075-0_12.
[42] de Jong PH, Salvatori Y, Libonati F, Mirzaali MJ, Zadpoor AA. Shape-locking in architected materials through 3D printed magnetically activated joints. Mater Des. 2023;235:112427. doi: 10.1016/j.matdes.2023.112427.
[43] Hassan H, Hallez H, Thielemans W, Vandeginste V. A review of electro-active shape memory polymer composites: Materials engineering strategies for shape memory enhancement. Eur Polym J. 2024;208:112861. doi: 10.1016/j.eurpolymj.2024.112861.
[44] Jamaludin AS, Najwa N, Mohd Zawawi MZ, Abdul Manaf AR, Hamidon R. State-of-the-art developments and perspectives on multifunctional magnetic soft composites (MMSCs). In: Abd. Aziz R, Ismail Z, Iqbal AKMA, Ahmed I, editors. Intelligent manufacturing and mechatronics. iM3F 2023. Springer proceedings in materials. Singapore: Springer. vol 40; 2024. p. 533–42.
[45] Kim H, Zan G, Seo Y, Lee S, Park C. Stimuli-responsive liquid metal hybrids for human-interactive electronics. Adv Funct Mater. 2024;34:2308703. doi: 10.1002/adfm.202308703.
[46] Kalva SN, Ali F, Velasquez CA, Koç M. 3D-printable PLA/Mg composite filaments for potential bone tissue engineering applications. Polymers (Basel). 2023;15(11):2572. doi: 10.3390/polym15112572.
[47] Ali F, Al Rashid A, Kalva SN, Koç M. Mg-Doped PLA composite as a potential material for tissue engineering—Synthesis, characterization, and additive manufacturing. Materials. 2023;16(19):6506. doi: 10.3390/ma16196506.
[48] A.S. D638-14, Standard test method for tensile properties of plastics 1, 2006. p. 1–15. 10.1520/D0638-14.1.
[49] Petcharoen K, Sirivat A. Magneto-electro-responsive material based on magnetite nanoparticles/polyurethane composites. Mater Sci Eng: C. 2016;61:312–23. doi: 10.1016/j.msec.2015.12.014.
[50] Thummarungsan N, Sirivat A. Magneto-responsive biopolymer composite based on plasticized poly(butylene succinate-co-butylene adipate) and Fe_3O_4 for flexible actuator application. J Polym Env. 2024;32:3246–57. doi: 10.1007/s10924-024-03190-z.
[51] Al Rashid A, Al-Maslamani NA, Abutaha A, Hossain M, Koç M. Cobalt iron oxide ($CoFe_2O_4$) reinforced polyvinyl alcohol (PVA) based magnetoactive polymer nanocomposites for remote actuation. Mater Sci Eng: B. 2025;311:117838. doi: 10.1016/j.mseb.2024.117838.